

A hydrogeomorphological index of heavy-tailed flood behavior

H. -J. Wang¹, R. Merz^{1,2}, S. Yang³, and S. Basso^{1,4}

¹Department of Catchment Hydrology, Helmholtz Centre for Environmental Research – UFZ, Halle (Saale), Germany,

²Institute of Geosciences and Geography, Martin-Luther University Halle-Wittenberg, Halle (Saale), Germany,

³Department of Aquatic Ecosystem Analysis, Helmholtz Centre for Environmental Research – UFZ, Magdeburg, Germany

⁴Norwegian Institute for Water Research (NIVA), Oslo, Norway

Corresponding author: Hsing-Jui Wang (hsing-jui.wang@ufz.de)

Key Points:

- The hydrograph recession exponent is identified as an index of heavy-tailed flood behavior.
- The proposed index enables robust identification of heavy-tailed flood behavior in a large set of case studies and from short data records.
- Unlike other frequently used metrics, the proposed index infers heavy-tailed flood behaviors from commonly observed discharge dynamics.

22 **Abstract**

23 Floods are often disastrous due to underestimation of the magnitude of rare events. When the
24 occurrence of floods follows a heavy-tailed distribution the chance of extreme events is sizable.
25 However, identifying heavy-tailed flood behavior is challenging because of limited data records
26 and the lack of physical support for currently used indices. We address these issues by deriving a
27 new index of heavy-tailed flood behavior from a physically-based description of streamflow
28 dynamics. The proposed index, which is embodied by the hydrograph recession exponent, enables
29 inferring heavy-tailed flood behavior from daily flow records. We test the index in a large set of
30 case studies across Germany. Results show its ability to identify cases with either heavy- or
31 nonheavy-tailed flood behavior, and to evaluate the tail heaviness. Remarkably, the results are
32 robust also for decreasing the lengths of data records. The new index thus allows for assessing
33 flood hazards from commonly available data.

34 **Plain Language Summary**

35 High flow events often cause severe damages when they occur unexpectedly, i.e., more often and
36 with larger magnitudes than suggested by historical observations. This is usually the case with
37 frequency distributions of floods which are heavy-tailed. However, a proper assessment of the tail
38 behavior solely based on limited data records is difficult and might lead to an erroneous estimation
39 of the underlying hazard. We start by analyzing runoff generation processes and find that the
40 hydrograph recession is a proper descriptor of the emergence of heavy-tailed behavior. Our
41 findings show that the new proposed index allows for (1) detecting cases with heavy-tailed
42 behavior, (2) comparing severity across cases, and (3) displaying robust results also with short data
43 records. These results address the main limitations of currently used metrics (which often require
44 long records and lack physical meaning) and provide information on the characteristic flood hazard
45 of river basins.

46 **1 Introduction**

47 Floods remain the leading natural hazards worldwide, which directly threaten at least one-fifth of
48 people's livelihoods (McDermott, 2022; Rentschler et al., 2022) and have caused enormous and
49 increasing economic losses (Bevere & Remondi, 2022) in recent years. Floods are often disastrous
50 because they occur unexpectedly (i.e., underestimated by water resources managers as well as
51 residents) (Else, 2021; Merz et al., 2021), commonly due to poor estimates of the magnitude of
52 rare events obtained from available observations. A number of studies in natural and anthropogenic
53 phenomena use heavy-tailed distributions to describe the extreme behavior of variables (e.g., Katz,
54 2002; Kondor et al., 2014; Malamud, 2004; Sartori & Schiavo, 2015; Wang et al., 2022) because
55 it indicates a sizable chance of the occurrence of extreme value. We can better assess the flood
56 hazards if we may know that floods follow a heavy-tailed distribution, i.e., robustly identify the
57 heavy-tailed flood behavior (Merz et al., 2022).

58 A variable distribution's tail heaviness is traditionally estimated graphically or mathematically,
59 while both have their limitations. In general, graphical methods such as log-log plots (Beirlant et
60 al., 2004), generalized Hill ratio plots (Resnick, 2007; El Adlouni et al., 2008), and mean excess
61 functions (Embrechts et al., 1997; Nerantzaki & Papalexiou, 2019) have less objectivity and
62 efficiency (Cooke et al., 2014). Mathematical methods provide more objective insights into the
63 estimation of tail behavior. The shape parameters of Generalized Extreme Value (GEV)

64 distributions quantify the tail behavior by fitting the parameters of an underlying distribution on
 65 limited records of maxima (Morrison & Smith, 2002; Villarini & Smith, 2010; Papalexiou et al.,
 66 2013), and a group of non-parametric metrics evaluates the spread of data (e.g., upper tail ratio
 67 (Lu et al., 2017; Smith et al., 2018; Villarini et al., 2011; Wang et al., 2022), Gini index (Eliazar
 68 & Sokolov, 2010; Rajah et al., 2014), and obesity index (Cooke & Nieboer, 2011; Sartori &
 69 Schiavo, 2015)). These methods often require long records to obtain reliable estimates (Papalexiou
 70 & Koutsoyiannis, 2013). This is a challenge globally and even more challenging when it comes to
 71 analyzing maxima (which is indeed the key to assessing hazards of extreme floods). The bias
 72 caused by the data size restricts the comparability across sites with different record lengths
 73 (Wietzke et al., 2020). In addition, the correctness of the estimation of tail heaviness is influenced
 74 by the underlying physical processes of the case studies (Merz et al., 2022). However, to the best
 75 of our knowledge, physical processes are absent from these frequently used metrics. It is preferable
 76 to have a new index that can robustly estimate with data in different lengths (Bernardara et al.,
 77 2008; Merz & Blöschl, 2009) and is based on the physical processes that favor the heavy-tailed
 78 behavior of flood distributions.

79 We propose a new index of heavy-tailed flood behavior, which can be estimated by common
 80 discharge dynamics. Unlike fitting a statistical distribution to observed series of maxima (which
 81 may not clearly exhibit heavy-tailed behavior due to data scarcity), the index infers the tail
 82 heaviness of floods by examining the intrinsic dynamics of the hydrological system. Reliable
 83 identification of heavy tails by the proposed index is tested in datasets with decreasing lengths in
 84 a great number of case studies with various climate and physiographic features. We leverage
 85 common discharge dynamics to facilitate flood peril assessment and demonstrate its usefulness in
 86 areas with limited records.

87 **2 Identifying tail behavior from hydrological dynamics**

88 We describe key hydrologic dynamics occurring at the catchment scale and the resulting
 89 probability distributions of streamflow and floods by means of the P_Hysically-based Extreme
 90 Value (PHEV) distribution of river flows (Basso et al., 2021). This framework is grounded on a
 91 well-established mathematical description of precipitation, soil moisture, and runoff generation in
 92 river basins (Laio et al., 2001; Porporato et al., 2004; Botter et al., 2007b, 2009). Rainfall is
 93 described as a marked Poisson process with frequency λ_p [T^{-1}] and exponentially distributed
 94 depths with average α [L]. Soil moisture increases due to rainfall infiltration and decreases due to
 95 evapotranspiration. The latter is represented by a linear function of soil moisture between the
 96 wilting point and an upper critical value expressing the water holding capacity of the root zone.
 97 Runoff pulses occur with frequency $\lambda < \lambda_p$ when the soil moisture exceeds the critical value.
 98 These pulses replenish single catchment storage, which drains according to a nonlinear storage-
 99 discharge relation. The related hydrograph recession is described via a power law function with
 100 exponent a [–] and coefficient K [L^{1-a}/T^{2-a}] (Brutsaert & Nieber, 1977), which allows for
 101 mimicking the joint effect of different flow components (Basso et al., 2015). Such a description of
 102 runoff generation and streamflow dynamics was successfully tested in a variety of hydro-climatic
 103 and physiographic conditions (Arai et al., 2020; Botter et al., 2007a; Botter et al., 2010; Ceola et

104 al., 2010; Doulatyari et al., 2015; Mejía et al., 2014; Müller et al., 2014; Müller et al., 2021; Pumo
 105 et al., 2014; Santos et al., 2018; Schaepli et al., 2013).

106 PHEV provides a set of consistent expressions for the probability distributions of daily streamflow,
 107 ordinary peak flows (i.e., local flow peaks occurring as a result of streamflow-producing rainfall
 108 events; Zorzetto et al., 2016), and floods (i.e., flow maxima in a certain timeframe; Basso et al.,
 109 2021). For example, the probability distribution of daily streamflow q can be expressed as (Botter
 110 et al., 2009):

$$111 \quad p(q) = C_1 \cdot q^{-a} \left(e^{\frac{-1}{\alpha K(2-a)} q^{2-a}} \right) \left(e^{\frac{\lambda}{K(1-a)} q^{1-a}} \right) \quad (1)$$

113 where C_1 is a normalization constant.

114 Taking the limit of Equation (1) for $q \rightarrow +\infty$ gives indications of the tail behavior of the flow
 115 distribution (Basso et al., 2015). This is determined by the three terms in the equation, namely, one
 116 power law and two exponential functions, which behave differently depending on the value of the
 117 hydrograph recession exponent a (Equation 2; notice that $a > 1$ in most natural river basins; Tashie
 118 et al., 2020a).

$$119 \quad \lim_{q \rightarrow +\infty} p(q) = \lim_{q \rightarrow +\infty} \left\{ C_1 \cdot q^{-a} \left(e^{\frac{-1}{\alpha K(2-a)} q^{2-a}} \right) \left(e^{\frac{\lambda}{K(1-a)} q^{1-a}} \right) \right\} \quad (2)$$

$$\begin{array}{ccccccc} & \mapsto 0 & & \mapsto 0 & & \mapsto e^0 = 1 & \text{for } 1 < a < 2 \\ & \underbrace{\hspace{1.5cm}} & \underbrace{\hspace{1.5cm}} & \underbrace{\hspace{1.5cm}} & & & \\ \lim_{q \rightarrow +\infty} p(q) = \lim_{q \rightarrow +\infty} \left\{ C_1 \cdot q^{-a} \left(e^{\frac{-1}{\alpha K(2-a)} q^{2-a}} \right) \left(e^{\frac{\lambda}{K(1-a)} q^{1-a}} \right) \right\} & & & & & & \\ & \underbrace{\hspace{1.5cm}} & \underbrace{\hspace{1.5cm}} & \underbrace{\hspace{1.5cm}} & & & \\ & \mapsto 0 & & \mapsto e^0 = 1 & & \mapsto e^0 = 1 & \text{for } a > 2 \end{array}$$

121 When $1 < a < 2$, the last term on the right-hand side converges to a constant value of one as q
 122 increases, thereby no more influence on how the distribution decreases toward zero. The first two
 123 terms instead decrease toward zero, affecting how the probability decreases for increasing values
 124 of q . The tail behavior is in this case determined by both a power law and an exponential functions,
 125 indicating that the probability decreases faster than an exponential but slower than a power law.
 126 When $a > 2$, both the exponential terms converge to a constant value of one as q increases, and
 127 thus no more influence on how the probability decreases toward zero. In this case the tail of the
 128 distribution is solely determined by the power law function. Despite being aware that several
 129 definitions of heavy-tailed distribution exist (El Adlouni et al., 2008; Vázquez et al., 2006), in the
 130 remaining of the manuscript we refer to heavy-tailed behavior for the case of distributions which
 131 exhibit a power law tail (i.e., the cases with $a > 2$). We thus aim to distinguish them from cases

132 which display a lighter tail because of the simultaneous effect of exponential decay (i.e., the cases
133 with $1 < a < 2$).

134 From the above derivations, the hydrograph recession exponent emerges as a key index of the tail
135 behavior of streamflow distributions, which shall be heavy-tailed for values of $a > 2$. The same
136 analysis applies to infer the tail behavior of the probability distributions of ordinary peak flows
137 (Botter et al., 2009) and floods (Basso et al., 2016) (see supporting information Text S1).
138 Remarkably, we find that the same critical value of the recession exponent indicates the emergence
139 of heavy-tailed behavior also in peak flow and flood distributions. We therefore propose the
140 hydrograph recession exponent a as an index for identifying heavy-tailed flood behavior, and test
141 its capability to correctly predict such behavior in Section 4.

142 Recent studies showed that the hydrograph recession exponent is a convincing descriptor of the
143 geomorphological signature of drainage areas (Biswal & Marani, 2010, 2014; Biswal & Kumar,
144 2014; Ghosh et al., 2016; Mutzner et al., 2013). The river network structure primarily defines how
145 the geometry of saturated (Mutzner et al., 2013) and unsaturated areas (Biswal & Marani, 2010)
146 of a river basin change over the draining process, which essentially determines the streamflow
147 dynamics at the outlet. Despite being aware of the influences of seasonal climate (Jachens et al.,
148 2020; Tashie et al., 2019), the geomorphological structure of the contributing river network has
149 been demonstrated as the major determinant of the hydrograph recession exponent (Biswal &
150 Kumar, 2014; Ghosh et al., 2016). We thus refer to the hydrograph recession exponent for a
151 hydrogeomorphological index of heavy-tailed flood behavior.

152 **3 Data and parameter estimation**

153 To test the proposed hydrogeomorphological index of heavy-tailed flood behavior (i.e., the
154 hydrograph recession exponent a), we use streamflow records with daily time resolution of 98
155 gauges across Germany (Figure S1). The analyzed river basins encompass a variety of climate and
156 physiographic settings (Tarasova et al., 2020), while not being heavily affected by anthropogenic
157 flow regulation and snow dynamics across seasons. Their areas range from 110 to 23,843 km² with
158 a median value of 1,195 km². The minimum, median, and maximum lengths of the streamflow
159 records are 35, 58, and 63 years (inbetween 1951 – 2013). We perform all analyses on a seasonal
160 basis (winter: December–February, spring: March–May, summer: June–August, fall: September–
161 November) to account for the seasonality of the hydrograph recessions and flood distributions
162 (Durrans et al., 2003; Tashie et al., 2020b). This results in an overall number of 386 case studies
163 used in our study.

164 We estimated a as the median value of the exponents of power law functions fitted to $dq/dt - q$
165 pairs of each hydrograph recession observed in the daily flow series (Jachens et al., 2020; Biswal,
166 2021). Notice that the proposed indicator of heavy-tailed flood behavior is thus estimated based
167 on commonly available daily discharge observations.

168 The identification of case studies with either heavy- or nonheavy-tailed behavior resulting from
169 the proposed index must be evaluated against a suitable benchmark. This is obtained by means of
170 a state-of-the-art approach to fit power law functions to empirical distributions and evaluate their
171 plausibility for the analyzed data (Clauzet et al., 2009). The fitted exponent is here noted as b . We
172 analyze three types of empirical data, namely daily streamflow, ordinary peaks, and monthly

173 maxima (Fischer & Schumann, 2016; Malamud & Turcotte, 2006), and obtain estimates of the
 174 fitted exponent b for each case. These results will be used to validate the capabilities of the
 175 proposed hydrogeomorphological index to infer heavy-tailed flood behavior from the analysis of
 176 hydrograph recessions.

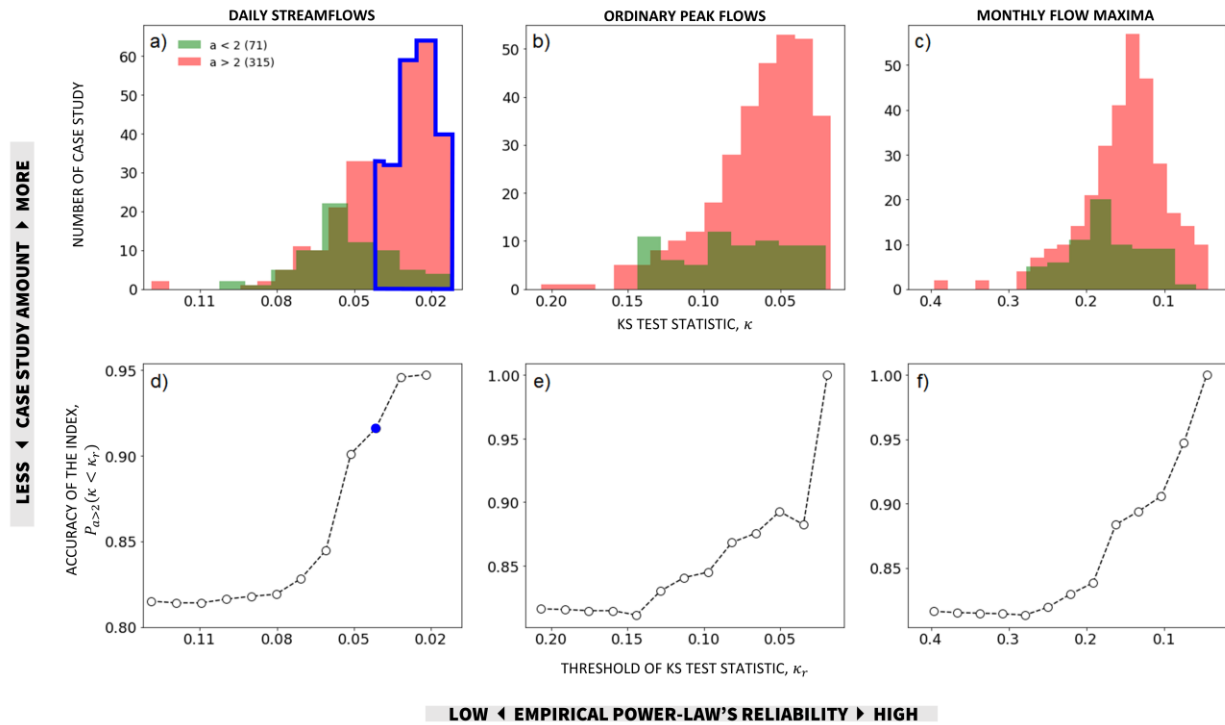
177 **4 Results and discussion**

178 We examine if power law distributions fitted to the empirical distributions of daily streamflow,
 179 ordinary peaks, and monthly maxima well describe the observed data for the case studies identified
 180 as having heavy-tailed behavior (i.e., $a > 2$) according to the hydrogeomorphological index (Figure
 181 1). First, we identify the case studies with either heavy- ($a > 2$; red) or nonheavy ($a < 2$; green) -
 182 tailed behavior based on the hydrogeomorphological index. Then, we use the Kolmogorov-
 183 Smirnov (KS) statistic κ to evaluate the reliability of the fitted power law function in describing
 184 the data ($\kappa \in [0, \infty]$, $\kappa = 0$ denotes the highest reliability). The KS statistic κ indicates how likely the
 185 data are to be drawn from a power law. Figures 1a-1c show that the histograms of the number of
 186 case studies are significantly skewed toward lower values of κ for all cases of daily streamflows,
 187 ordinary peak flows, and monthly flow maxima with $a > 2$ (red histograms), whereas this is not
 188 true for cases with $a < 2$ (green histograms). Statistical significance of the skewnesses was
 189 evaluated through the Jarque–Bera test at a significance level of 0.05. The result essentially
 190 indicates that data from case studies which are identified with heavy-tailed behavior according to
 191 the hydrogeomorphological index ($a > 2$, red) are indeed more likely to come from power law
 192 distributions.

193 We further estimate the accuracy of the hydrogeomorphological index based on the fraction of
 194 case studies that are correctly identified by the hydrogeomorphological index among all heavy-
 195 tailed cases. To define the number of cases with heavy tails based on the available observations,
 196 we choose a threshold value of κ to determine whether the data are reliably described by power
 197 law functions. Mathematically, the accuracy can be expressed as $P_{a > 2}(\kappa < \kappa_r) = N_p(a > 2)/N_p$,
 198 where κ_r is the imposed threshold of κ , N_p is the number of case studies whose $\kappa < \kappa_r$, and
 199 $N_p(a > 2)$ is the number of case studies with $a > 2$ among the N_p case studies. Higher accuracy
 200 essentially means that a higher fraction of heavy-tailed cases (as defined by fitted power laws and
 201 a set κ_r threshold) are correctly identified by means of the hydrogeomorphological index. Notice
 202 that the smaller the κ_r threshold, the more reliable the description of power law distributions for
 203 data. The blue frame and dot in figures 1a and 1d display an example of defined reliability and the
 204 corresponding accuracy.

205 Figures 1d-1f display the accuracy of the hydrogeomorphological index as a function of the
 206 reliability threshold κ_r . In all three cases (daily streamflows, ordinary peak flows, and monthly
 207 flow maxima), the accuracy values increase with the reliability level of the power law function
 208 fitted on observed data. This means that the hydrogeomorphological index shows higher accuracy
 209 for case studies where the empirical distributions of observed data are more consistent with power
 210 laws. In other words, the proposed hydrogeomorphological index, which is estimated as the

211 hydrograph recession exponent from commonly available daily flow records, is a robust indicator
 212 of heavy-tailed flood behavior.



213
 214 **Figure 1. Accuracy of the proposed hydrogeomorphological index.** (a)-(c) Number of analyzed case
 215 studies as a function of the KS statistic κ of empirically fitted power law distributions (the latter is a measure
 216 of how reliable the power law is as a model for the given data: the lower κ , the more reliable the power law
 217 model). Case studies are identified with either heavy- ($a > 2$, red histograms) or nonheavy ($a < 2$, green
 218 histograms) –tailed behavior based on the hydrograph recession exponent
 219 a estimated from daily flow records, which is proposed as a hydrogeomorphological index of heavy-
 220 tailed streamflow and flood behavior. (d)-(f) Accuracy of the hydrogeomorphological index as a function
 221 of decreasing thresholds of κ_r (i.e., increasing reliability of empirical power laws). The accuracy $P_{a>2}(\kappa <$
 222 $\kappa_r)$ is essentially the fraction of the red area under a specified threshold of κ (as explanatorily shown by
 223 the blue frames and dots in panels a and d). The values of the KS statistic κ are derived from records of (a,
 224 d) daily streamflows, (b, e) ordinary peak flows, and (c, f) monthly flow maxima.

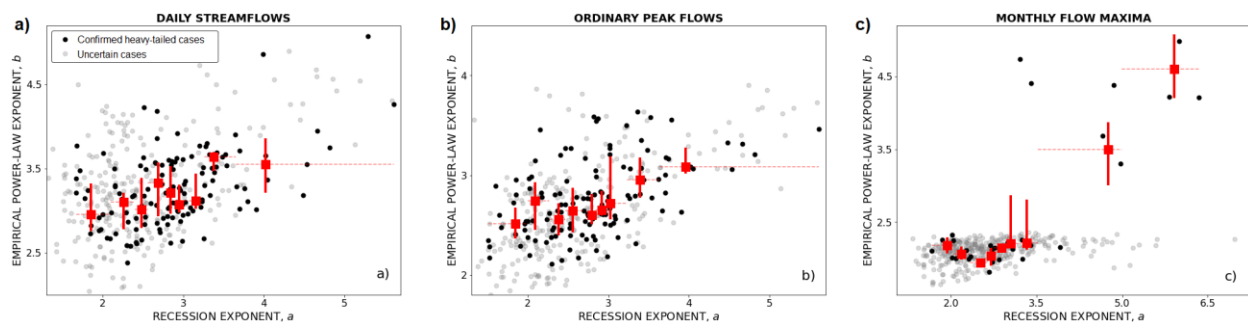
225 We further employ the goodness-of-fit testing procedure proposed by Clauset et al. (2009)
 226 (supporting information Text S2) to identify case studies for which the representation of daily
 227 streamflow, ordinary peak flows, and monthly maxima by means of power law distributions is
 228 convincingly supported by the available data. We refer to these case studies as ‘confirmed heavy-
 229 tailed cases’ (Figure 2, black dots). Conversely, we term the remaining ones as ‘uncertain cases’
 230 (Figure 2, gray). The latter label denotes that the distribution underlying the available observations
 231 may or may not be a power law but, statistically speaking, we cannot be conclusive due to data
 232 scarcity.

233 Figure 2 shows the empirical power law exponent b as a function of the hydrogeomorphological
 234 index of heavy-tailed flow behavior a . Red markers display the median values of a and b (squares),
 235 the interquartile intervals of b (vertical bars), and the binning ranges of a (horizontal bars, equal

236 number of case studies in each bin), highlighting the correlation between the empirical power law
 237 exponent b and the hydrograph recession exponent a for confirmed heavy-tailed cases (black dots)
 238 in all three cases (i.e., daily streamflows, ordinary peak flows, and monthly flow maxima). We
 239 also test the correlation by calculating their distance correlation (Székely et al., 2007), which is
 240 valid for both potential linear and nonlinear associations between two random variables. We find
 241 that a and b are significantly correlated at a significance level of 0.05 in all three cases with
 242 distance (Spearman) correlation coefficients of 0.45, 0.44, and 0.81 (0.42, 0.46, and 0.60) for daily
 243 streamflows, ordinary peak flows, and monthly flow maxima. The last high value of correlation is
 244 likely affected by the existence of two clusters of black dots in Figure 2c. Nonetheless, the
 245 existence of a statistically significant correlation between the empirical power law exponent and
 246 the hydrogeomorphological index (confirmed for all panels a,b,c) confirms that the latter not only
 247 can be used to identify heavy-tailed flood behavior but also to evaluate the degree of the tail
 248 heaviness of the underlying distributions.

249 Figure 2c is of particular interest because it shows a common issue in the practice of flood hazard
 250 assessment. The power law is a plausible representation of the empirical distribution of monthly
 251 maxima in some cases (black dots) that are characterized by large values of the recession exponent
 252 a and are therefore classified as having heavy-tailed behavior according to the
 253 hydrogeomorphological index. In other cases (gray dots), conclusive evidence of possible heavy-
 254 tailed flood behavior cannot be drawn from the limited observations of monthly maxima. However,
 255 the hydrogeomorphological index retains its capability to provide estimates of the tail heaviness
 256 based on the value of the hydrograph recession exponent and classifies the case studies as heavy-
 257 tailed. Such a classification is deemed robust, provided that the predictions of the
 258 hydrogeomorphological index are confirmed by observations in cases (panels a and b) where data
 259 size is not a limitation (i.e., for daily streamflow and ordinary peak flows). The ability of the
 260 hydrogeomorphological index to infer the tail heaviness of flood distributions by examining the
 261 intrinsic dynamics of the hydrological system constitutes an advantage of the approach, that is
 262 especially useful in the very common cases when the tail of the flood distribution cannot be known
 263 from limited observations of maxima only.

264



265

266 **Figure 2. Empirical power law exponent b as a function of the hydrogeomorphological index of**
 267 **heavy-tailed behavior a .** Case studies are classified into groups of confirmed heavy-tailed (black dots)
 268 and uncertain (gray dots) cases on the basis of the goodness-of-fit testing procedure (Clauset et al., 2009).
 269 The former denotes cases for which a power law provides a reliable description of the empirical data
 270 distribution, while the latter denotes cases whose data cannot convincingly support such a distribution. Red
 271 markers highlight the correlation between the empirical power law exponent b and the hydrograph recession
 272 exponent a for confirmed heavy-tailed cases in the case of (a) daily streamflows ($n=121$ case studies), (b)
 273 ordinary peak flows ($n=116$), and (c) monthly flow maxima ($n=34$). Red markers display the median values

274 of a and b (squares), the interquartile intervals of b (vertical bars), and the binning ranges of a (horizontal
275 bars, equal number of case studies in each bin).

276 In Figure 3, we test the index stability of the categorization of case studies into heavy/nonheavy-
277 tailed flood behavior for decreasing data lengths. We benchmark the hydrogeomorphological
278 index (i.e., the hydrograph recession exponent a) against two other frequently used metrics of
279 heavy tails in hydrological studies: (1) the upper tail ratio (UTR) (Lu et al., 2017; Smith et al.,
280 2018; Villarini et al., 2011; Wang et al., 2022) and (2) the shape parameter ξ of the GEV
281 distribution (Morrison & Smith, 2002; Papalexiou et al., 2013; Villarini & Smith, 2010). The UTR
282 is derived as the ratio of the maximum record to the 0.9 quantiles of floods (Smith et al., 2018),
283 and the ξ is estimated using the python package OpenTURNS 1.16 (Baudin et al., 2017). We
284 compute both using data of monthly flow maxima. For all three indices (a , UTR, and ξ), we
285 estimate the index for decreasing data lengths from 35 (bounded by the shortest record length in
286 the dataset) to 2 years in each case study. The index for each test length is calculated based on the
287 median value of the estimates derived from 30 random fragments (with the assigned test length)
288 of the entire record.

289 To have the reference of the stability of the categorization, we use the entire data record computing
290 the values of the hydrogeomorphological index and the GEV shape parameter (notations with an
291 asterisk in Figure 3, i.e., a^* and ξ^*). Each case study is categorized as either having (red) or not
292 (green) the heavy-tailed behavior by the criteria of heavy (nonheavy) tails for the
293 geomorphological index as $a^* > 2$ ($a^* < 2$) or for the GEV shape parameter as $\xi^* > 0$ ($\xi^* \leq 0$)
294 (Godrèche et al., 2015). For the UTR, however, there is no specific threshold for the identification
295 of heavy/nonheavy tails, but a larger value indicates a heavier tail.

296 The categorization of the hydrogeomorphological index is consistent across the test data length
297 (Figure 3a). Specifically, the index estimates retain beyond 2 for most heavy-tailed cases (red) and
298 below 2 for most nonheavy-tailed cases (green) when the data length decreases. The vertical
299 shaded bar and line show the 0.25–0.75 and 0.05–0.95 quantile ranges of the index estimates across
300 case studies. Besides the consistent categorization, the index estimates vary in a narrow range over
301 the test data length both for the median value (i.e., from 2.64 to 2.92 for heavy-tailed cases and
302 from 1.84 to 2.0 for nonheavy-tailed cases) and for the variation (e.g., the coefficient of variation
303 ranges from 0.29 to 0.33 for heavy-tailed cases and from 0.29 to 0.33 for nonheavy-tailed cases).
304 The small fluctuation of the variation across the test data length implies that the variation in index
305 estimates is primarily caused by case study heterogeneity rather than decreasing data length. These
306 results essentially confirm the stability of the hydrogeomorphological index for decreasing data
307 lengths.

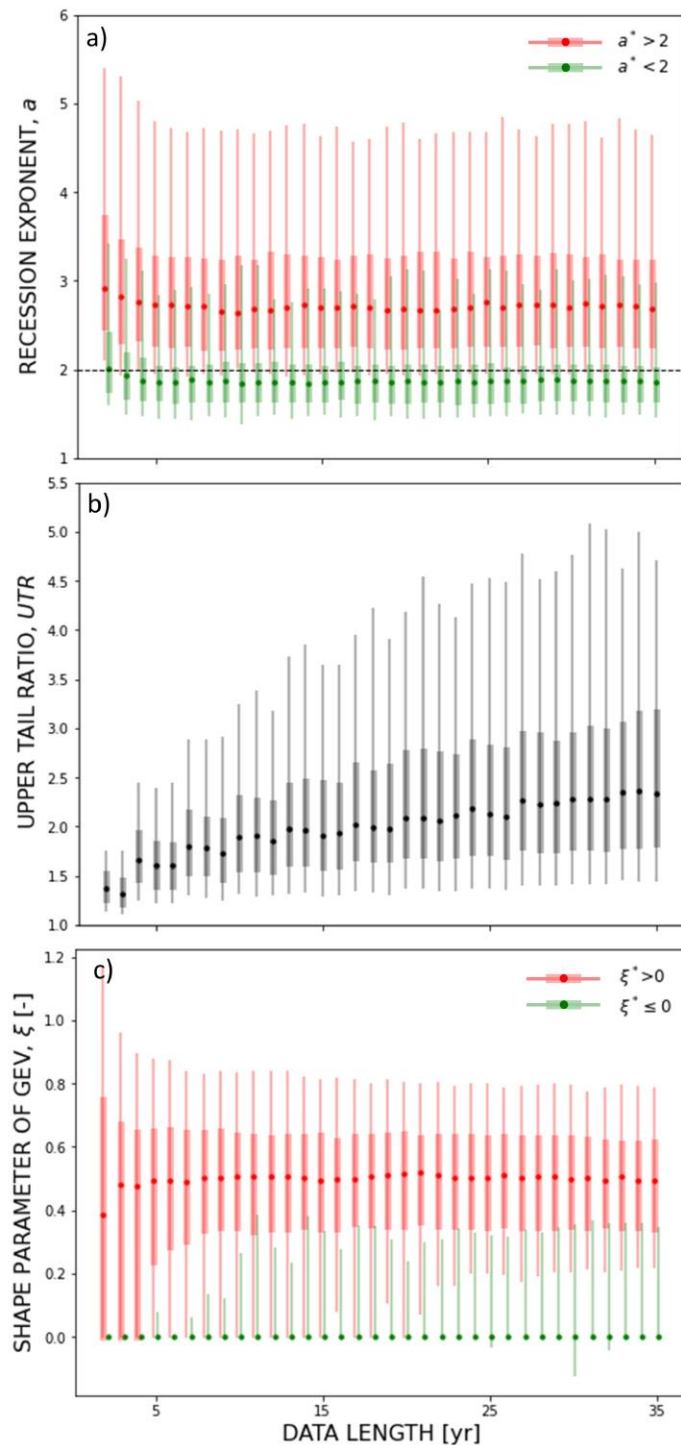
308 In contrast, the upper tail ratio shows pronounced instability for decreasing data lengths (Figure
309 3b). The median value of the index estimates ranges from 1.32 to 2.36, and the coefficient of
310 variation ranges from 0.15 to 0.64, indicating that the tail heaviness is underestimated as data
311 length decreases, in agreement with Smith et al. (2018) and Wietzke et al. (2020). The differential
312 variation for decreasing data length denotes an apparent bias in the index estimates caused by the
313 short data in addition to the heterogeneity across case studies.

314 Figure 3c shows the categorization of tail behavior based on the estimates of the GEV shape
315 parameters. When the test data length is above five years, case studies with index estimates in the

316 interquartile range (the vertical shaded bar) are consistent in the categorization of heavy/nonheavy-
317 tailed behavior. When the data length is below five years, the underestimation of tail heaviness
318 exists. Meanwhile, the index estimate changes slightly in its median but evidently in its coefficient
319 of variation across the test data length. The former (latter) ranges from 0.39 to 0.52 (0.37 to 1.03)
320 for the heavy-tailed cases and keeps 0 (--; the coefficient of variation is not applied for data with
321 zero mean) for the nonheavy-tailed cases. These results show that the GEV shape parameter may
322 still be considered a practical index for the heavy/nonheavy-tailed categorization because most
323 applications have data that are more than five years. Nonetheless, the bias in the variation of index
324 estimates across data length and the apparent underestimation in cases with very limited data point
325 to the dependence on data lengths, in agreement with Papalexiou and Koutsoyiannis (2013).

326 We demonstrate the hydrogeomorphological index is robust in cases with limited data, i.e., it is
327 stable in the categorization of heavy/nonheavy-tailed flood behavior for decreasing data lengths.
328 Given that most data records worldwide are relatively short (Lins, 2008), this is a valuable tool to
329 infer the tail behavior of streamflow in river basins. Moreover, given that generally all available
330 records are too short of estimating the tail behavior of maxima (e.g., floods), this approach is even

331 more valuable because it allows scientists or engineers to estimate the heavy-tailed flood behavior
 332 and assess the hazards from common discharge dynamics.



333

334 **Figure 3. Stability of the categorization of case studies into heavy/nonheavy-tailed flood behavior for**
 335 **decreasing data lengths.** Estimates of three different indices of tail behavior as a function of data length.
 336 (a) Hydrograph recession exponent a (i.e., the proposed hydrogeomorphological index of this study). Two
 337 frequently used metrics of heavy tails in hydrological studies: (b) the upper tail ratio UTR , and (c) the shape

338 parameter ξ of the GEV distribution. Dots display the median values of the estimates for 386 case studies;
339 vertical shaded bars and lines respectively show the 0.25-0.75 and 0.05-0.95 quantile ranges of the estimates.
340 The entire data record was used for computing the reference values of the hydrograph recession exponent
341 α^* and the GEV shape parameter ξ^* and categorizing each case study as either having (red) or not (green)
342 the heavy-tailed behavior.

343 **5 Conclusions**

344 The hydrograph recession exponent is identified as an index of heavy-tailed flood behavior from
345 a physically-based description of hydrological dynamics. It is essentially a
346 hydrogeomorphological index of heavy-tailed flood behavior because it originates from the
347 geomorphological structure of the contributing river basin. We show that the proposed
348 hydrogeomorphological index enables the identification of heavy/nonheavy-tailed flood behavior
349 and the evaluation of the tail heaviness across case studies. Remarkably, it leverages the
350 information of common discharge dynamics and shows robust identification of tail behavior for
351 decreasing data length. We demonstrate all these capabilities in a large set of case studies across
352 Germany on a seasonal basis, featuring the diversity in climatic and physiographic conditions. The
353 hydrogeomorphological index addresses the limitations of other frequently used indices (e.g., lack
354 of physical support, low effectiveness/ineffectiveness in cases with limited data) and allows for
355 robust identification of heavy-tailed flood behavior, which is particularly useful in assessing
356 hazards of extreme floods in data-scarce areas.

357 **Acknowledgments**

358 This work is funded by the Deutsche Forschungsgemeinschaft-Project 421396820 “Propensity of
359 rivers to extreme floods: climate-landscape controls and early detection (PREDICTED)” and FOR
360 2416 “Space-Time Dynamics of Extreme Floods (SPATE)”. The financial support of the
361 Helmholtz Centre for Environmental Research and the Norwegian Institute for Water Research is
362 as well acknowledged. SY (the 3rd author) acknowledges the support of the Helmholtz Climate
363 Initiative Project funded by the Helmholtz Association. The manuscript and supporting
364 information provide all the information needed to replicate the results.

365 **Data Availability Statement**

366 For providing the discharge data for Germany, we are grateful to the Bavarian State Office of
367 Environment (LfU, <https://www.gkd.bayern.de/de/fluesse/abfluss>) and the Global Runoff Data
368 Centre (GRDC) prepared by the Federal Institute for Hydrology (BfG, <http://www.bafg.de/GRDC>).
369 Climatic data can be obtained from the German Weather Service (DWD;
370 <ftp://ftp-cdc.dwd.de/pub/CDC/>). The digital elevation model can be retrieved from Shuttle Radar
371 Topography Mission (SRTM; <https://cgiarcsi.community/data/srtm-90m-digital-elevation-database-v4-1/>).

372

373

374

375

376 **References**

- 377 Arai, R., Toyoda, Y., & Kazama, S. (2020). Runoff recession features in an analytical
 378 probabilistic streamflow model. *Journal of Hydrology*, *597*, 125745.
 379 <https://doi.org/10.1016/j.jhydrol.2020.125745>
- 380 Basso, S., Botter, G., Merz, R., & Miniussi, A. (2021). PHEV! The PHysically-based Extreme
 381 Value distribution of river flows. *Environmental Research Letters*, *16*(12).
 382 <https://doi.org/10.1088/1748-9326/ac3d59>
- 383 Basso, S., Schirmer, M., & Botter, G. (2015). On the emergence of heavy-tailed streamflow
 384 distributions. *Advances in Water Resources*, *82*, 98–105.
 385 <https://doi.org/10.1016/j.advwatres.2015.04.013>
- 386 Basso, S., Schirmer, M., & Botter, G. (2016). A physically based analytical model of flood
 387 frequency curves. *Geophysical Research Letters*, *43*(17), 9070–9076.
 388 <https://doi.org/10.1002/2016GL069915>
- 389 Baudin, M., Dutfoy, A., Iooss, B., & Popelin, A.-L. (2017). OpenTURNS: An Industrial
 390 Software for Uncertainty Quantification in Simulation BT - Handbook of Uncertainty
 391 Quantification. In R. Ghanem, D. Higdon, & H. Owhadi (Eds.) (pp. 2001–2038). Cham:
 392 Springer International Publishing. https://doi.org/10.1007/978-3-319-12385-1_64
- 393 Beirlant, J., Goegebeur, Y., Teugels, J., Segers, J., De Waal, D., & Ferro, C. (2004). *Statistics of*
 394 *extremes: Theory and applications*. Wiley.
 395 <https://doi.org/https://doi.org/10.1002/0470012382>
- 396 Bernardara, P., Schertzer, D., Sauquet, E., Tchiguirinskaia, I., & Lang, M. (2008). The flood
 397 probability distribution tail: How heavy is it? *Stochastic Environmental Research and Risk*
 398 *Assessment*, *22*(1), 107–122. <https://doi.org/10.1007/s00477-006-0101-2>
- 399 Bevere, L., & Remondi, F. (2022). *Natural catastrophes in 2021: the floodgates are open*. Swiss
 400 *Re Institute sigma research*.
- 401 Biswal, B. (2021). Decorrelation is not dissociation: There is no means to entirely decouple the
 402 Brutsaert-Nieber parameters in streamflow recession analysis. *Advances in Water*
 403 *Resources*, *147*, 103822. <https://doi.org/https://doi.org/10.1016/j.advwatres.2020.103822>
- 404 Biswal, B., & Marani, M. (2010). Geomorphological origin of recession curves. *Geophysical*
 405 *Research Letters*, *37*(24), 1–5. <https://doi.org/10.1029/2010GL045415>
- 406 Biswal, B., & Marani, M. (2014). “Universal” recession curves and their geomorphological
 407 interpretation. *Advances in Water Resources*, *65*, 34–42.
 408 <https://doi.org/10.1016/j.advwatres.2014.01.004>

- 409 Biswal, B., & Nagesh Kumar, D. (2014). What mainly controls recession flows in river basins?
410 *Advances in Water Resources*, 65, 25–33. <https://doi.org/10.1016/j.advwatres.2014.01.001>
- 411 Botter, G., Basso, S., Porporato, A., Rodriguez-Iturbe, I., & Rinaldo, A. (2010). Natural
412 streamflow regime alterations: Damming of the Piave river basin (Italy). *Water Resources*
413 *Research*, 46(6), 1–14. <https://doi.org/10.1029/2009WR008523>
- 414 Botter, G., Peratoner, F., Porporato, A., Rodriguez-Iturbe, I., & Rinaldo, A. (2007). Signatures of
415 large-scale soil moisture dynamics on streamflow statistics across U.S. climate regimes.
416 *Water Resources Research*, 43(11), 1–10. <https://doi.org/10.1029/2007WR006162>
- 417 Botter, G., Porporato, A., Rodriguez-Iturbe, I., & Rinaldo, A. (2007). Basin-scale soil moisture
418 dynamics and the probabilistic characterization of carrier hydrologic flows: Slow, leaching-
419 prone components of the hydrologic response. *Water Resources Research*, 43(2), 1–14.
420 <https://doi.org/10.1029/2006WR005043>
- 421 Botter, G., Porporato, A., Rodriguez-Iturbe, I., & Rinaldo, A. (2009). Nonlinear storage-
422 discharge relations and catchment streamflow regimes. *Water Resources Research*, 45(10),
423 1–16. <https://doi.org/10.1029/2008WR007658>
- 424 Brutsaert, W., & Nieber, J. L. (1977). Regionalized drought flow hydrographs from a mature
425 glaciated plateau. *Water Resources Research*, 13(3), 637–643.
426 <https://doi.org/10.1029/WR013i003p00637>
- 427 Ceola, S., Botter, G., Bertuzzo, E., Porporato, A., Rodriguez-Iturbe, I., & Rinaldo, A. (2010).
428 Comparative study of ecohydrological streamflow probability distributions. *Water*
429 *Resources Research*, 46(9), 1–12. <https://doi.org/10.1029/2010WR009102>
- 430 Clauset, A., Shalizi, C. R., & Newman, M. E. J. (2009). Power-law distributions in empirical
431 data. *SIAM Review*, 51(4), 661–703. <https://doi.org/10.1137/070710111>
- 432 Cooke, R. M., Nieboer, D., & Misiewicz, J. (2014). *Fat-Tailed Distributions: Data, Diagnostics*
433 *and Dependence* (volume 1). John Wiley & Sons.
- 434 Cooke, R. M., & Nieboer, D. (2011). Heavy-Tailed Distributions: Data, Diagnostics, and New
435 Developments. *Resources for the Future Discussion Paper, No. 11-19*.
436 <https://doi.org/dx.doi.org/10.2139/ssrn.1811043>
- 437 Doulatyari, B., Betterle, A., Basso, S., Biswal, B., Schirmer, M., & Botter, G. (2015). Predicting
438 streamflow distributions and flow duration curves from landscape and climate. *Advances in*
439 *Water Resources*, 83, 285–298. <https://doi.org/10.1016/j.advwatres.2015.06.013>
- 440 Durrans, S. R., Eiffe, M. A., Thomas, W. O., & Goranflo, H. M. (2003). Joint Seasonal /Annual
441 Flood Frequency Analysis. *Journal of Hydrologic Engineering*, 8(4), 181–189.
442 [https://doi.org/10.1061/\(asce\)1084-0699\(2003\)8:4\(181\)](https://doi.org/10.1061/(asce)1084-0699(2003)8:4(181))

- 443 El Adlouni, S., Bobée, B., & Ouarda, T. B. M. J. (2008). On the tails of extreme event
444 distributions in hydrology. *Journal of Hydrology*, 355(1–4), 16–33.
445 <https://doi.org/10.1016/j.jhydrol.2008.02.011>
- 446 Eliazar, I., & Sokolov, I. (2010). Gini characterization of extreme-value statistics. *Physica A-
447 Statistical Mechanics and Its Applications - PHYSICA A*, 389, 4462–4472.
448 <https://doi.org/10.1016/j.physa.2010.07.005>
- 449 Else, H. (2021). Climate change implicated in Germany’s deadly floods. *Nature*.
450 <https://doi.org/10.1038/d41586-021-02330-y>
- 451 Embrechts, P., Klüppelberg, C., & Mikosch, T. (1997). *Modelling extreme events for insurance
452 and finance*. Springer Berlin Heidelberg.
- 453 Fischer, S., & Schumann, A. (2016). Robust flood statistics: comparison of peak over threshold
454 approaches based on monthly maxima and TL-moments. *Hydrological Sciences Journal*,
455 61(3), 457–470. <https://doi.org/10.1080/02626667.2015.1054391>
- 456 Ghosh, D. K., Wang, D., & Zhu, T. (2016). On the transition of base flow recession from early
457 stage to late stage. *Advances in Water Resources*, 88, 8–13.
458 <https://doi.org/10.1016/j.advwatres.2015.11.015>
- 459 Godrèche, C., Majumdar, S. N., & Schehr, G. (2015). Statistics of the longest interval in renewal
460 processes. *Journal of Statistical Mechanics: Theory and Experiment*, 2015(3).
461 <https://doi.org/10.1088/1742-5468/2015/03/P03014>
- 462 Jachens, E. R., Rupp, D. E., Roques, C., & Selker, J. S. (2020). Recession analysis revisited:
463 Impacts of climate on parameter estimation. *Hydrology and Earth System Sciences*, 24(3),
464 1159–1170. <https://doi.org/10.5194/hess-24-1159-2020>
- 465 Katz, R. (2002). Statistics of Extremes in Climatology and Hydrology. *Advances in Water
466 Resources*, 25, 1287–1304.
- 467 Kondor, D., Pósfai, M., Csabai, I., & Vattay, G. (2014). Do the rich get richer? An empirical
468 analysis of the Bitcoin transaction network. *PLoS ONE*, 9(2).
469 <https://doi.org/10.1371/journal.pone.0086197>
- 470 Laio, F., Porporato, A., Fernandez-Illescas, C. P., & Rodriguez-Iturbe, I. (2001). Plants in water-
471 controlled ecosystems: Active role in hydrologic processes and response to water stress IV.
472 Discussion of real cases. *Advances in Water Resources*, 24(7), 745–762.
473 [https://doi.org/10.1016/S0309-1708\(01\)00007-0](https://doi.org/10.1016/S0309-1708(01)00007-0)
- 474 Lins, H. F. (2008). Challenges to hydrological observations. *WMO Bulletin*, 57(January), 55–58.

- 475 Lu, P., Smith, J. A., & Lin, N. (2017). Spatial characterization of flood magnitudes over the
476 drainage network of the Delaware river basin. *Journal of Hydrometeorology*, 18(4), 957–
477 976. <https://doi.org/10.1175/JHM-D-16-0071.1>
- 478 Malamud, B. D. (2004). Tails of natural hazards. *Physics World*, 17(8), 31–35.
479 <https://doi.org/10.1088/2058-7058/17/8/35>
- 480 Malamud, B. D., & Turcotte, D. L. (2006). The applicability of power-law frequency statistics to
481 floods. *Journal of Hydrology*, 322(1–4), 168–180.
482 <https://doi.org/10.1016/j.jhydrol.2005.02.032>
- 483 McDermott, T. K. J. (2022). Global exposure to flood risk and poverty. *Nature Communications*,
484 13(1), 6–8. <https://doi.org/10.1038/s41467-022-30725-6>
- 485 Mejía, A., Daly, E., Rossel, F., Javanovic, T., & Gironás, J. (2014). A stochastic model of
486 streamflow for urbanized basins. *Water Resources Research*, 50, 1984–2001.
487 <https://doi.org/10.1002/2013WR014834>
- 488 Merz, B., Basso, S., Fischer, S., Lun, D., Blöschl, G., Merz, R., et al. (2022). Understanding
489 heavy tails of flood peak distributions. *Water Resources Research*, 1–37.
490 <https://doi.org/10.1029/2021wr030506>
- 491 Merz, B., Blöschl, G., Vorogushyn, S., Dottori, F., Aerts, J. C. J. H., Bates, P., et al. (2021).
492 Causes, impacts and patterns of disastrous river floods. *Nature Reviews Earth and*
493 *Environment*, 2(9), 592–609. <https://doi.org/10.1038/s43017-021-00195-3>
- 494 Merz, R., & Blöschl, G. (2009). Process controls on the statistical flood moments - a data based
495 analysis. *Hydrological Processes*, 23(5), 675–696. <https://doi.org/10.1002/hyp>
- 496 Morrison, J. E., & Smith, J. A. (2002). Stochastic modeling of flood peaks using the generalized
497 extreme value distribution. *Water Resources Research*, 38(12), 41-1-41–12.
498 <https://doi.org/10.1029/2001wr000502>
- 499 Müller, M. F., Dralle, D. N., & Thompson, S. E. (2014). Analytical model for flow duration
500 curves in seasonally dry climates. *Water Resources Research*, 50, 5510–5531.
501 <https://doi.org/10.1002/2014WR015301>
- 502 Müller, M. F., Roche, K. R., & Dralle, D. N. (2021). Catchment processes can amplify the effect
503 of increasing rainfall variability. *Environmental Research Letters*, 16(8).
504 <https://doi.org/10.1088/1748-9326/ac153e>
- 505 Mutzner, R., Bertuzzo, E., Tarolli, P., Weijs, S. V., Nicotina, L., Ceola, S., et al. (2013).
506 Geomorphic signatures on Brutsaert base flow recession analysis. *Water Resources*
507 *Research*, 49(9), 5462–5472. <https://doi.org/10.1002/wrcr.20417>

- 508 Nerantzaki, S. D., & Papalexiou, S. M. (2019). Tails of extremes: Advancing a graphical method
509 and harnessing big data to assess precipitation extremes. *Advances in Water Resources*, 134.
510 <https://doi.org/10.1016/j.advwatres.2019.103448>
- 511 Papalexiou, S. M., Koutsoyiannis, D., & Makropoulos, C. (2013). How extreme is extreme? An
512 assessment of daily rainfall distribution tails. *Hydrology and Earth System Sciences*, 17(2),
513 851–862. <https://doi.org/10.5194/hess-17-851-2013>
- 514 Papalexiou, S. M., & Koutsoyiannis, D. (2013). Battle of extreme value distributions : A global
515 survey on extreme daily rainfall. *Water Resources Research*, 49(1), 187–201.
516 <https://doi.org/10.1029/2012WR012557>
- 517 Porporato, A., Daly, E., & Rodriguez-Iturbe, I. (2004). Soil water balance and ecosystem
518 response to climate change. *American Naturalist*, 164(5), 625–632.
519 <https://doi.org/10.1086/424970>
- 520 Pumo, D., Viola, F., La Loggia, G., & Noto, L. V. (2014). Annual flow duration curves
521 assessment in ephemeral small basins. *Journal of Hydrology*, 519(PA), 258–270.
522 <https://doi.org/10.1016/j.jhydrol.2014.07.024>
- 523 Rajah, K., O’Leary, T., Turner, A., Petrakis, G., Leonard, M., & Westra, S. (2014). Changes to
524 the temporal distribution of daily precipitation. *Geophysical Research Letters*, 41(24),
525 8887–8894. <https://doi.org/10.1002/2014GL062156>
- 526 Rentschler, J., Salhab, M., & Jafino, B. A. (2022). Flood exposure and poverty in 188 countries.
527 *Nature Communications*, 13(1), 3527. <https://doi.org/10.1038/s41467-022-30727-4>
- 528 Resnick, S. I. (2007). *Heavy-Tail Phenomena: Probabilistic and Statistical Modeling*. New
529 York: Springer US.
- 530 Santos, A. C., Portela, M. M., Rinaldo, A., & Schaepli, B. (2018). Analytical flow duration
531 curves for summer streamflow in Switzerland. *Hydrology and Earth System Sciences*, 22(4),
532 2377–2389. <https://doi.org/10.5194/hess-22-2377-2018>
- 533 Sartori, M., & Schiavo, S. (2015). Connected we stand: A network perspective on trade and
534 global food security. *Food Policy*, 57, 114–127.
535 <https://doi.org/https://doi.org/10.1016/j.foodpol.2015.10.004>
- 536 Schaepli, B., Rinaldo, A., & Botter, G. (2013). Analytic probability distributions for snow-
537 dominated streamflow. *Water Resources Research*, 49(5), 2701–2713.
538 <https://doi.org/10.1002/wrcr.20234>
- 539 Smith, J. A., Cox, A. A., Baeck, M. L., Yang, L., & Bates, P. (2018). Strange Floods: The Upper
540 Tail of Flood Peaks in the United States. *Water Resources Research*, 54(9), 6510–6542.
541 <https://doi.org/10.1029/2018WR022539>

- 542 Székely, G. J., Rizzo, M. L., & Bakirov, N. K. (2007). Measuring and testing dependence by
543 correlation of distances. *Annals of Statistics*, 35(6), 2769–2794.
544 <https://doi.org/10.1214/0090536070000000505>
- 545 Tarasova, L., Basso, S., & Merz, R. (2020). Transformation of Generation Processes From Small
546 Runoff Events to Large Floods. *Geophysical Research Letters*, 47(22).
547 <https://doi.org/10.1029/2020GL090547>
- 548 Tashie, A., Pavelsky, T., & Band, L. E. (2020). An Empirical Reevaluation of Streamflow
549 Recession Analysis at the Continental Scale. *Water Resources Research*, 56(1), 1–18.
550 <https://doi.org/10.1029/2019WR025448>
- 551 Tashie, A., Pavelsky, T., & Emanuel, R. E. (2020). Spatial and Temporal Patterns in Baseflow
552 Recession in the Continental United States. *Water Resources Research*, 56(3), 1–18.
553 <https://doi.org/10.1029/2019WR026425>
- 554 Tashie, A., Scaife, C. I., & Band, L. E. (2019). Transpiration and subsurface controls of
555 streamflow recession characteristics. *Hydrological Processes*, 33(19), 2561–2575.
556 <https://doi.org/10.1002/hyp.13530>
- 557 Vázquez, A., Oliveira, J. G., Dezsö, Z., Goh, K. Il, Kondor, I., & Barabási, A. L. (2006).
558 Modeling bursts and heavy tails in human dynamics. *Physical Review E - Statistical,*
559 *Nonlinear, and Soft Matter Physics*, 73(3), 1–19.
560 <https://doi.org/10.1103/PhysRevE.73.036127>
- 561 Villarini, G., & Smith, J. A. (2010). Flood peak distributions for the eastern United States. *Water*
562 *Resources Research*, 46(6), 1–17. <https://doi.org/10.1029/2009WR008395>
- 563 Villarini, G., Smith, J. A., Baeck, M. L., Marchok, T., & Vecchi, G. A. (2011). Characterization
564 of rainfall distribution and flooding associated with U.S. landfalling tropical cyclones:
565 Analyses of Hurricanes Frances, Ivan, and Jeanne (2004). *Journal of Geophysical Research*
566 *Atmospheres*, 116(23). <https://doi.org/10.1029/2011JD016175>
- 567 Wang, H., Merz, R., Yang, S., Tarasova, L., & Basso, S. (2022). Emergence of heavy tails in
568 streamflow distributions: the role of spatial rainfall variability. *Advances in Water*
569 *Resources Journal*, 171(104359). <https://doi.org/10.1016/j.advwatres.2022.104359>
- 570 Wietzke, L. M., Merz, B., Gerlitz, L., Kreibich, H., Guse, B., Castellarin, A., & Vorogushyn, S.
571 (2020). Comparative analysis of scalar upper tail indicators. *Hydrological Sciences Journal*,
572 65(10), 1625–1639. <https://doi.org/10.1080/02626667.2020.1769104>
- 573 Zorzetto, E., Botter, G., & Marani, M. (2016). On the emergence of rainfall extremes from
574 ordinary events. *Geophysical Research Letters*, 43(15), 8076–8082.
575 <https://doi.org/10.1002/2016GL069445>